Study of Attapulgite as an Additive in Reinforced Concrete by Substitution of Cement and Its Effects on the Durability Properties of Hardened Concrete

Malang Bodian[1,2], Dame Keinde[3], Ismaila Yade[1], Kinda Hannawi[2], Prince William Agbodjan[2], Modou Fall[1]* , Aveline Darquennes[2]*

[1]Organic Physical Chemistry and Environmental Analysis Laboratory (LCPOAE), Chemistry Department, Cheikh Anta Diop University, Dakar, Senegal
[2]Laboratoire de Génie Civil et Génie Mécanique (LGCGM), Université de Rennes, INSA Rennes, Rennes, France
[3]Civil Engineering Materials Laboratory (LMGC), Higher Plytechnic School, Cheikh Anta Diop University, Dakar, Senegal
Email: bodianthomas@gmail.com, dame.keinde@ucad.edu.sn, ismala.yade@yahoo.fr, Kinda.Hannawi@insa-rennes.fr, William.Prince-Agbodjan@insa-rennes.fr, *modou.fall@ucad.edu.sn, aveline.darquennes@insa-rennes.fr

Abstract

The valorization of Senegalese attapulgite clay in concrete, as a solution against the exhaustion of the cement deposits was studied. In that purpose, attapulgite was first calcined at 800°C to make it reactive and added in concrete by substitution of Portland cement (CEM I 52.5N) at contents of 0, 5 and 10% by conserving a constant water/cement ratio value of 0.65. The effects of the partial replacement of cement by attapulgite on the physicochemical and mechanical properties of the concrete as well as on the steel-concrete bond were examined. For this purpose, the water porosity, the intrinsic permeability and the density of the clay-based concrete were evaluated. Compression, tensile and pull-out tests were carried out to determine the impact of clay on the Young modulus, the compressive and tensile strengths and the steel-concrete bond. This study was completed by a characterization of the pozzolanic reactivity of calcined attapulgite. All the results of these studies were compared with those of Portland cement as a reference. The substitution of cement by attapulgite up to 10% in concrete has only a small influence on its porosity and permeability and confers to the concrete gain in compressive strength of 11%. However, it caused a loss of steel-concrete bond of 10%.

Keywords

Attapulgite, Concrete, Mechanical Properties, Pozzolanic Reactivity, Reinforced

Concrete

1. Introduction

Steel concrete is the most widely used construction material in the world. However, concerns about the depletion of cement deposits are increasingly being raised (Reference [1]). It is therefore essential to save cement deposits by reducing cement usage. A practical strategy to reduce cement consumption is to replace cement with locally available supplementary materials. The most popular of these include fly ash, silica fume and slag. However, calcined clay is nowadays considered as a main substitute for cement because of its pozzolanic activity, its abundance and its wide availability (Reference [2] [3]). According to Liu *et al.*, (Reference [4]) kaolinite has the highest pozzolanic content followed by montmorillonite and illite. However, the limited availability of high-grade kaolin clay deposits and its high price are obstacles to its widespread application in the cement industry. Thus, the use of low-grade kaolinic clays as substitute materials for cement is becoming an alternative. For example, Alujas *et al.* (Reference [5]) revealed that clays with moderate kaolinite content (40%) are a potential source of pozzolan which is highly reactive with cement materials. Calcined clay with low kaolin content favors the formation of hydrated calcium monosulfoaluminate (AFm) with longer chains. In addition to improving concrete quality, studies have shown that partial replacement of cement by calcined clays can provide significant benefits in terms, enhanced resistance to chemical attack, corrosion inhibition for reinforced concrete, and reduced alkaline reactions with aggregates (Reference [6] [7] [8] [9] [10]). The research of Vejmelkova *et al.* (Reference [11]) found that 10% metakaolin (MK) substitution is required as the amount needed to enhance certain properties of MK-based concrete mixtures or simply to ensure the level of quality compared to portland cement-based concrete. These works confirmed the possibility of using calcined clays as partial substitutes for cement in order to obtain good quality concrete. However, at present, no study on attapulgite as a partial substitute for cement has been carried out. This is why our interest was focused on this material, which is found in abundance and near Dakar, in order to valorize it in reinforced concrete as a substitute for cement.

Therefore, this study aims at evaluating the effect of attapulgite on the properties of concrete and on steel-concrete bonding in the hardened state. To this end, the influence of attapulgite on the physicochemical properties (water porosity, intrinsic permeability and density) of concrete was evaluated. Then its impact on the Young modulus and on the tensile and compressive strengths of concrete were determined. At the same time, the pozzolanic reactivity of attapulgite was also evaluated. Finally, the influence of attapulgite on the steel-concrete bond was studied. The use of attapulgite as additive in concrete and as a cement subs-

titute is particularly important for Senegal and other countries that have large quantities of this clay in order to reduce the consumption of cement deposits.

2. Experimental

2.1. Materials and Concrete Manufacturing Preparation

Attapulgite (Att) is introduced in the concrete under study as a substitute for cement at contents ranging from 5% to 10% for cement production costs reduction purposes. The clay originates from Pout (Senegal), and its chemical composition is given in Table 1 (Reference [10]).

Table 1 shows that the sum of percentages of Al_2O_3, SiO_2 and Fe_2O_3 is higher than 70%. According to the work of Amandine (Reference [12]), its activity index I = 0.9. This means, according to ASTM C618, that attapulgite could have pozzolanic characteristics. In addition, the difference between the silica content and that of lime is greater than 34%, which means that this material is acidic and contains a glassy phase, so it is possible to fix the lime released by the cement.

Before its use in the formulation of reinforced concrete, attapulgite was ground to 80 μm powder and then calcined in a kiln at the temperature of 800°C. Its particle size curve is presented in Figure 1. The cooking rate was set at 5°C per minute.

Calcination is an essential step in the development of a man-made pozzolan from a clay, as it allows the transition from a crystalline structure (an ordered arrangement of atoms) to an amorphous structure (a disordered structure of atoms). After calcination of attapulgite, a change in the color of the materials was observed (Figure 2), which means a change in the state of constitution, because the evaporation of water and the change of some minerals deteriorate the mesh of these minerals.

Table 1. Chemical composition of attapulgite (Reference [10]).

Name	Chemical elements (%)					
	SiO₂	Al₂O₃	Fe₂O₃	MgO	Ignition loss	CaO
Attapulgite	57%	13%	2%	14%	11.4%	-------
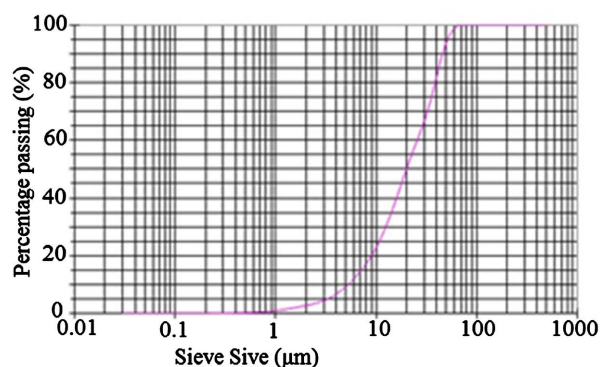
Figure 1. Laser particle size curve of attapulgite calcined at 800°C.

(a)

(b)

Figure 2. (a) Attapulgite in its natural state; (b) Attapulgite in its crushed and calcined state.

Table 2. Formulation (kg/m³) of the concrete.

Materials	Witness	5% Att	10% Att
Cement CEM I 52.5N	270	256.5	243
Gravel 4/10	1031	1031	1031
Sand 0/4	940	940	940
Water	175.5	180.2	185
Attapulgite	0	13.5	27
E/C = 0.65			

Attapulgite is substituted in concrete while keeping the Water/Cement ratio constant as shown in Table 2. However, due to its high water absorption capacity which can be up to 180% of its mass, water is compensated in the mix design up to 100% of its mass. This compensated amount of water (100% of the clay weight) gives the same slumps as the reference concrete.

The concrete and reinforced concrete specimens were made from this formulation and some of them contain clay. They are then kept in a humid room at 95% RH and 20˚C just after their confection. After their demolding, after 24 hours, the specimens are subjected to a wet cure by immersion in water until 90 days. The reinforced concrete specimens used for the pull-out tests were cylindrical, 130 mm high and 110 mm in diameter, and were made using the formulation described above (see Figure 3). The dimensions of the test specimen are those recommended by of the French standard NF EN 10080 (Reference [13]) in Annex D. The reinforcements used in the making of these reinforced concretes are high bond steels with a diameter of 12 mm.

2.2. Experimental Tests and Methods

- **Water porosity and intrinsic permeability**

Water-accessible porosity measures the percentage of voids connected with the surface, within the mass of the material. It measures the communicative or open porosity of the material reachable by water. The porosity is defined by the

ratio between the volume of voids accessible to water and the total volume of the material. After 90 days of wet cure under water, the water-accessible porosity (P_w) measurements were carried out on cylindrical specimens of 110 mm diameter and 50 mm height. After the wet cure, the specimens were first subjected to vacuum for 4 hours and then saturated with water under vacuum for 48 hours. The apparent volume of the specimen is determined by weighing the saturated specimen in air (M_{air}) and in water (M_w) at 0.01%. The samples are then dried in an oven at 105°C until the mass is stabilized to obtain the dry mass (M_{dry}). The mass is considered constant when the difference between the values obtained after two successive weighings (24 h interval) is less than 0.05% (Reference [14]). The porosity accessible to water is calculated according to Equation (1):

$$P_w = \frac{M_{air} - M_{dry}}{M_{air} - M_w} \times 100 \tag{1}$$

The intrinsic permeability measurement was performed on the same specimens used for porosity tests. After drying them subsequently to the porosity test in the oven at 105°C until constant mass, the helium permeability test started immediately. Helium was used as percolating medium for all gas permeability measurements. This choice is justified by the low atomic mass of this gas (4.003 g/mol), and its very small atomic radius (31×10^{-12} m) which allows it to percolate in the finest pores. The approach consisted in keeping the containment pressure constant (8 bar) and varying the percolation pressure (P_x) from 1 to 5 bar. For each percolation pressure, the flow rate (Q) was measured every 15 minutes until a constant value was reached.

For each pressure, the apparent permeability (K_a) was calculated from the following formula (Reference [15]):
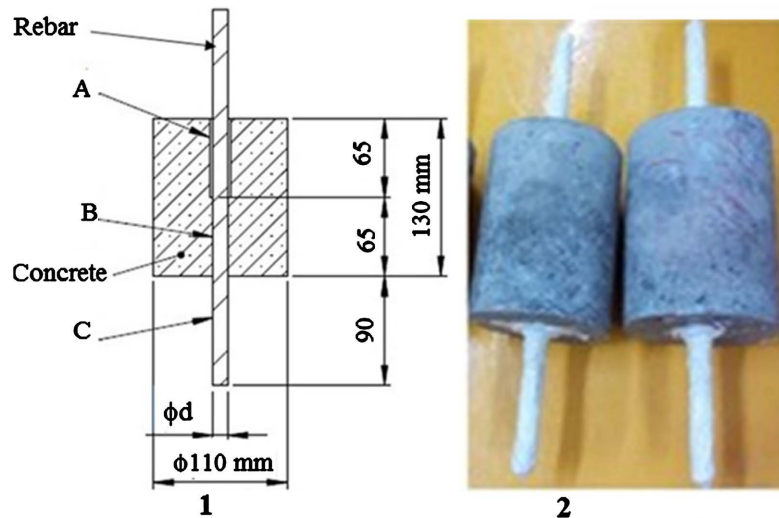
Figure 3. 1) Geometry of the samples used for electrochemical and pull-out test tests. A: Non adherent part; B: Part of the reinforcement anchored in the concrete; C: Part of the continuous reinforcement, protected by an epoxy resin; 2) Images of reinforced concrete.

$$K_a = \frac{2 \cdot P_2 \cdot Q \cdot L \cdot \mu}{A \cdot \left(P_1^2 - P_2^2\right)} \qquad (2)$$

The intrinsic permeability K_v was then deduced from the apparent permeability according to the Klinkenberg approach (Reference [16]):

$$K_a = K_v \left(1 + \frac{\beta}{P_m}\right) \qquad (3)$$

where P_m is the average pressure, equal to $(P_1 + P_2)/2$, β the Klinkenberg coefficient, P_2 the absolute pressure at the outlet (Pa) and P_1 the absolute pressure at the inlet (Pa), L (50 mm) the length of the specimen traversed by the fluid and μ viscosity of helium at $20°C = 1.94 \times 10^{-5}$ Pa.s.

- **Compressive strength and Young modulus**

Uniaxial compression and longitudinal modulus of elasticity tests were performed at different curing ages of 3 days, 7 days, 28 days and 90 days under water. The tests were carried out on 110×220 mm × mm cylindrical specimens using a 3000KN Controlab press, working at a speed of 0.5 MPa/s in accordance with standard NF EN 12390-3. Before the compression tests, the specimens were ground on their upper and lower surfaces using a grinder. The device used to determine the Young modulus is shown on **Figure 4**. It contains circular rings centered up so that measurements were taken outside the area of the shrinkage cones. These rings were equipped with 3 longitudinal LVDT-type displacement transducers, arranged at an angle of 120°. A series of three loads was applied to the specimen. At each time, the specimen was loaded to 30% of the failure stress previously determined from the compressive strength tests. A loading rate of 0.5 MPa/s was applied.

The longitudinal modulus of elasticity was determined from Equation (4) (Reference [17] [18]):

$$E = \frac{\Delta\sigma}{\Delta\varepsilon} = \frac{\sigma_a - \sigma_b}{\varepsilon_a - \varepsilon_b} \qquad (4)$$
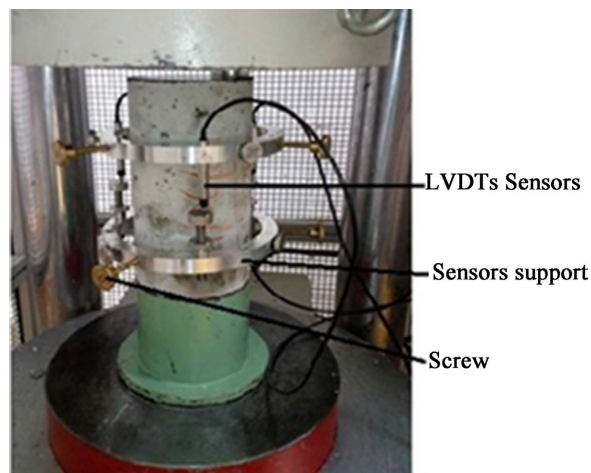
Figure 4. Device for determining the Young modulus.

where:

σ_a: 30% of the compressive strength (σ max)

σ_b: 5% of the compressive strength

ε_a: Average strain under stress σ_a

ε_b: Average strain under stress σ_b

- **Thermogravimetric analysis (TGA)**

Thermogravimetric analysis (TGA) is a technique in which variation of mass of a sample is measured when it is subjected to a temperature program, under controlled atmosphere. TGA was carried out using an equipment composed of a furnace (METLER TOLEDO) coupled to an acquisition system associated with the STARev.15 software. The principle consists in measuring the mass loss of a representative sample of about 60 - 70 mg, placed in a cylindrical crucible, during the rise in temperature to 1000˚C with a ramp of 10˚C/min. The samples were taken from concrete just after the simple compression test. They were then mechanically ground into powder and sieved to 80 μm. The resulting powder was mixed in alcohol to stop the hydration reaction. One hour later, the mixture was filtered and the series was repeated 3 times. At the end of this series, the sample was dried at 45˚C in a vacuum oven for 24 h before running the TGA test.

- **Pull-out test coupled with acoustic emission**

The pull-out test is a technique to evaluate the performance of the steel-concrete bond. The tests coupled with acoustic emission were carried out using a TESTOMETIC press with a capacity of 200 kN, controlled in displacement at a speed of 0.5 mm/min. The pull-out test consisted in applying a force on the reinforcement located in the upper (loaded) part of the specimen and the relative displacement between the steel and the concrete was measured at the unloaded end of the specimen using three LVDT displacement transducers (±2.5 mm travel) attached to the bar with rings (**Figure 5(a)**). The deformations of the concrete during loading were recorded by acoustic emissions using 6 piezoelectric sensors placed around the concrete surface (**Figure 5(a)** and **Figure 5(b)**). The sensors positioning on the surface of the specimen has an influence on the shape of the measured signal. This parameter must be studied according to the attenuation of the material but also according to the location of the damage. The configuration presented in **Figure 5(a)** was adopted, after several tests of sensor positioning configurations on the specimen. The six Nano30 sensors convert the waves into electrical signals which are connected to 2/4/6 preamplifiers with a gain of 20, 40 or 60 dB in a frequency band between 100 and 1000 kHz. Two sensors (1 and 2) are positioned in the bottom at a level of 10 mm height, two other sensors (5 and 6) are located on top, at a level of 120 mm and two sensors 3 and 4 are positioned in the middle (**Figure 5(b)**). The coordinates of the different sensors along the X, Y and Z axes are given in **Table 3**.

If the shear stresses (τ) are assumed to be uniformly distributed over the bond length, the ultimate average bond stresses are given by Equation (5) (Reference [19] [20] [21]):
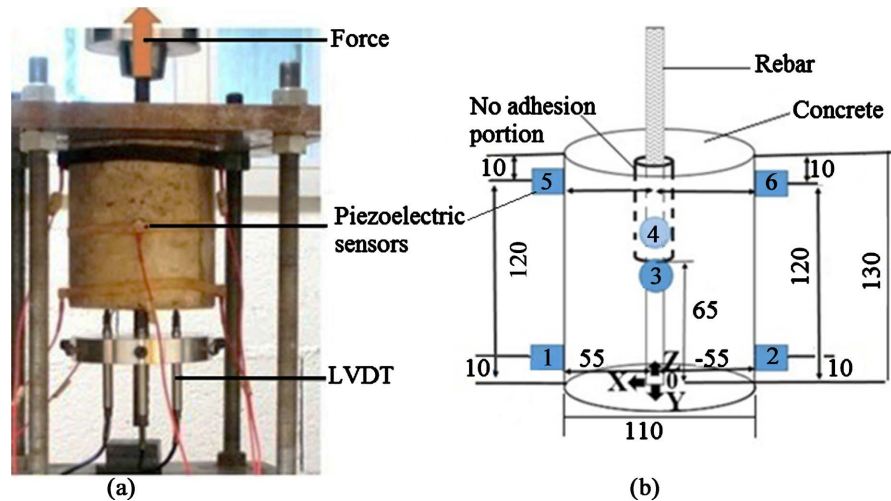
Figure 5. (a) Device of the pull-out test coupled with acoustic emission; (b) Position of the EA sensors placed on the surface of the specimen.

Table 3. Position of the acoustic sensors placed around the specimen.

Sensor numbers	Position of the sensors		
	X (mm)	Y (mm)	Z (mm)
Sensor 1	55	0	10
Sensor 2	−55	0	10
Sensor 3	0	55	65
Sensor 4	0	−55	65
Sensor 5	55	0	120
Sensor 6	−55	0	120

$$\tau = \frac{F_m}{d_a l_a \pi} \tag{5}$$

F_m is the maximum applied force (N), d_a is the diameter of the rebar (mm) and l_a is the anchored length (mm).

3. Results and Discussion

3.1. Effect of Attapulgite on Concrete Behavior

- **Physical and chemical properties of concrete**

The results of water accessible porosity and intrinsic permeability performed on three samples at 90 days of maturation are presented in **Figure 6(a)** and **Figure 6(b)**, respectively. The density values corresponding to the average of 3 samples of each given composition and determined at different maturation ages are presented in **Figure 6(c)**. At each given maturity, the measured values of porosity, intrinsic permeability and density are of the same order of magnitude for the different compositions. Indeed, we obtained an intrinsic permeability of
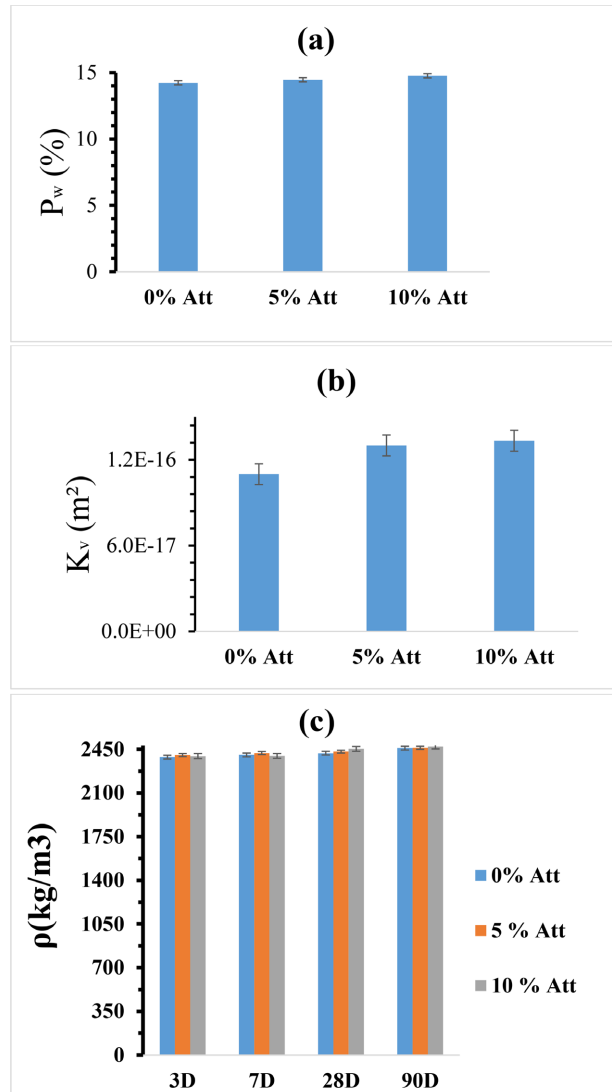
Figure 6. Influence of attapulgite on (a) water accessible porosity; (b) Intrinsic permeability and (c) Density of concrete with or without attapulgite.

1.10×10^{-16} for the reference, 1.30×10^{-16} for 5% attapulgite and 1.33×10^{-16} for 10% attapulgite. This negligible variation, after substitution of cement by attapulgite up to 10% suggested a filling of the voids by products resulting from a reaction between attapulgite and cement hydrates. For a given composition, the density increased only slightly with the age of the specimens (**Figure 6(c)**), reflecting a weak progress of the hydration reaction in the various compositions.

- **Mechanical properties of concrete**

The results are compared to the reference (0% attapulgite) at different maturation ages. For each sample, 3 specimens were tested. The different results of the compressive strength (f_c), tensile strength (f_t) and Young modulus (E) of the test bodies are presented in **Figure 7**.

Figure 7(a) and **Figure 7(b)** show a decrease in strength and Young modulus at 3 and 7 days of maturation with increasing attapulgite percentage, which can
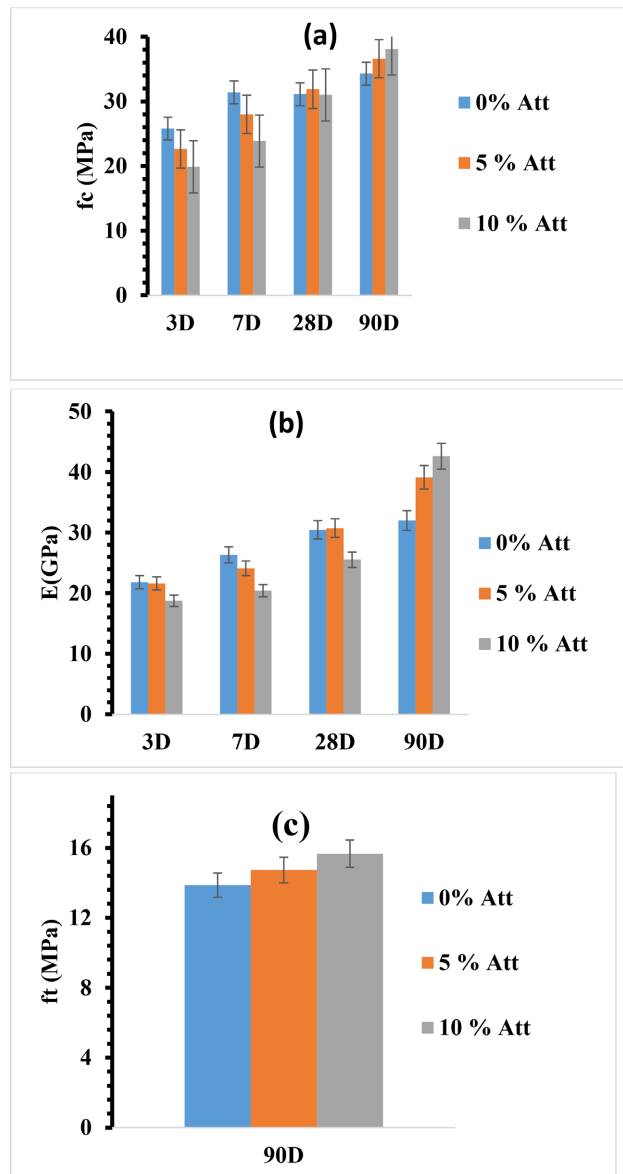
Figure 7. Influence of attapulgite addition on (a) Compressive strength; (b) Young modulus of elasticity and (c) Tensile strength.

be attributed to slow attapulgite activity. The compressive strength and modulus increase slightly compared to the reference at 28 days for the specimens containing 5% clay and at 90 days for those containing 10% clay. Thus, at 28 days, the value of the compressive strength is 31.1 MPa for the control, 31.9 MPa for the concrete with 5% attapulgite, and 31 MPa for the concrete with 10% attapulgite. At 90 days, it is 38.1 MPa for 10% attapulgite (*i.e.* an increase of 11.0%), 36.6 MPa for 5% clay addition (*i.e.* an increase of 6.7%) and 34.3 MPa for the control. This result confirms the work of Rashiddadash *et al* (Reference [22]), who showed an increase in the compressive strength of metakaolin-based concrete at higher ages. Benaissa *et al* (Reference [23]) also showed that the addition of bentonite calcined at 800˚C into the mortar improves the compressive strength

with age.

This opposite effect noted after 28 days and 90 days could be related to the formation of hydrates resulting from the interaction between the reactive silica in the glassy phase of the clay and the portlandite released by the hydration of the cement. **Figure 7(c)** shows a slight increase in tensile strength with clay substitution. To confirm the pozzolanic reaction of attapulgite, a thermogravimetric analysis (TGA) is performed on clay-containing specimens. The TGA curves of concrete containing or not attapulgite are presented in **Figure 8**.

The curves show 4 peaks, 3 of which correspond successively to the decomposition of the minerals in the sample during the test. The first peak appears at about 105˚C and corresponds to free water that can immediately evaporate. A second peak noted around 170˚C relates to the departure of chemically bound water present in the hydrates, attributable to the decomposition of calcium silicate hydrate (C-S-H). The formal identification of hydrate types remains difficult because of the overlapping peaks, as the dehydration temperature of a given mineral may vary according to the test conditions. A third peak is observed between 430˚C and 520˚C (depending on the test conditions) where the portlandite or calcium hydroxide (C-H) loses its water molecule to form quicklime. The last peak between 630˚C and 830˚C may be assigned to the release of carbon dioxide (CO_2) during the decomposition of calcite ($CaCO_3$) from different sources, notably that resulting from the carbonation of portlandite, or that initially present in the cement in the form of limestone filler, sand or clay.

This study is particularly devoted to the $Ca(OH)_2$ (portlandite) evolution as a function of the attapulgite substitution rate at different ages in order to estimate their pozzolanic reactivity. Indeed, when the hydration reaction of the clinker releases portlandite, the pozzolanic reaction consumes it. For this purpose, the total mass of portlandite in the sample at each age is determined by using the mass loss between 430˚C and 520˚C and by considering Equation (7).

$$Ca(OH)_2 \rightarrow CaO + H_2O$$
$$74\ \text{g/mol} \qquad 18\ \text{g/mol}$$

(6)
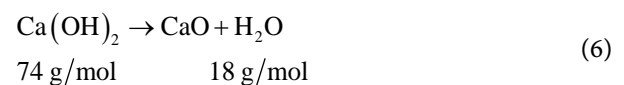
From Equation (6) it is obtained:

$$\%Ca(OH)_2 = \frac{m_{H_2O}}{m_i \times 18} \times 74 \times 100$$

$$\%Ca(OH)_2 = \frac{\%H_2O \times 74}{18}$$

(7)

With $\%H_2O = \dfrac{m_{H_2O}}{m_i} \times 100$, the relative mass loss recorded from the TGA curves.

The portlandite contents calculated using equation Equation (7) and from the mass lose recorded on the TGA curves between 430˚C and 520˚C (average values after 2 measurements) are presented in **Figure 9**.
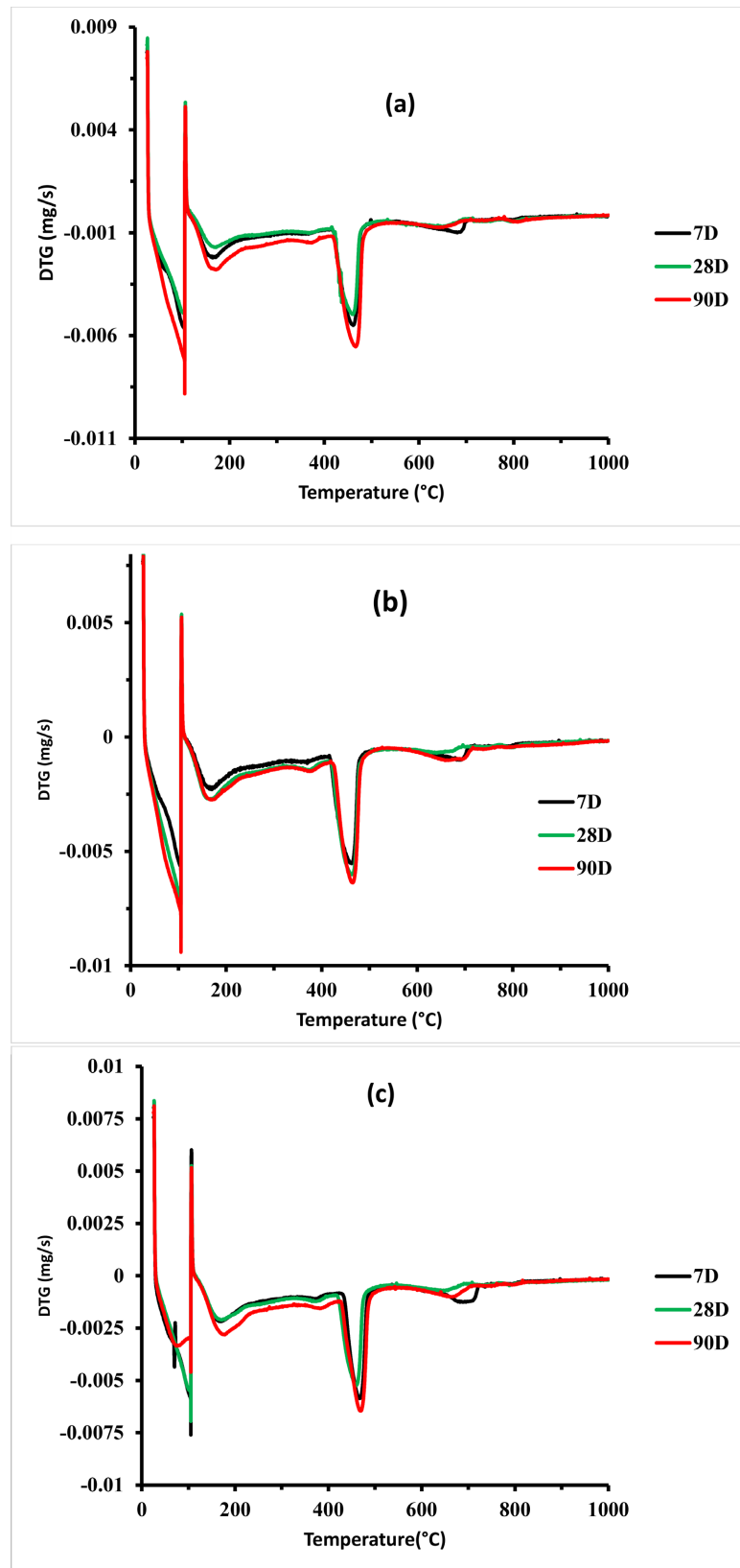
Figure 8. Derivative of the mass loss curve of the different composition samples: (a) Reference; (b) 5% attapulgite and (c) 10% attapulgite.
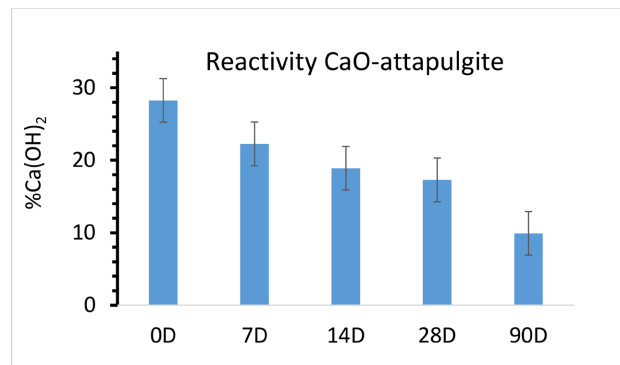
For the reference, the portlandite content increases with the maturation age. This increase with time reflects an advancement in the hydration of the mixtures (Reference [24]). For the formulations containing attapulgite, a slight decrease of the content with the age of maturation is observed. This decrease could be explained by a reactivity of portlandite with attapulgite. Attapulgite was then mixed with quicklime considering ratios of Lime/attapulgite = 2 and Water/Liant = 0.95 to verify this hypothesis of reactivity between the silica present in the glassy phase of attapulgite and portlandite. At each step, two samples were tested by TGA following the protocol described above. **Figure 10** shows the evolution of the portlandite content as a function of time. A progressive decrease of portlandite was noted, confirming the reaction between attapulgite and portlandite produced from the hydration of the cement.

3.2. Effect of Attapulgite on Steel Concrete Bond

In this section, we examine the effect of clay addition on steel-concrete bonding. Pull-out tests are performed after the 90-day wet cure. The curves showing the evolution of the bond stress of the clay-based reinforced concrete as a function
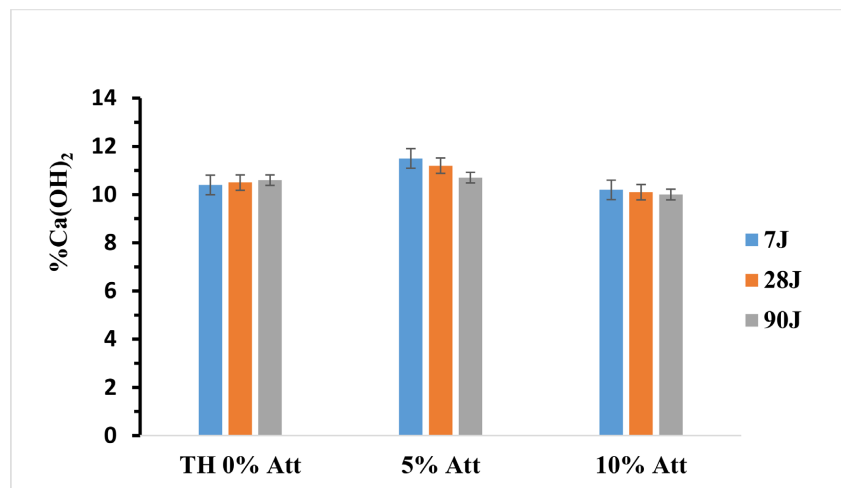
**Figure 9.** Portlandite content in different concretes at different times.

Figure 10. Portlandite content produced during the mixing of attapulgite with lime at different curing days.

of the slip of the bar recorded in the passive part are presented in Figure 11. The results are compared with the 100% cement reference specimen tested at 90 days of maturation (TH90).

Figure 11 shows that the initial phase (first slope at zero slip) corresponding to the cohesion between the bar and the concrete is influenced by the substitution of clay for cement. The slope is steeper in the case of clay specimens. The stress measured just before the detachment of the curve from the Y-axis also increases with the substitution rate of clay in the concrete. We note values of 1.69 MPa for the reference (TH 90D), 2.14 MPa for a 5% substitution (5% Att TH90D) and 5 MPa for 10% addition (10% Att TH90D). This evolution of the slope and of the bond stress could be explained by the formation of products resulting from the reaction between attapulgite and portlandite at the steel-concrete interface. The second slope (between the point of separation of the curve from the ordinate axis and the maximum of the curve) is steeper in the case of clay-based concrete. On the other hand, the bond stress (stress at the maximum of the curve) of clay-based concretes is lower compared to the reference. On the other hand, the reinforced concrete containing 10% clay has a better bond strength compared to the one composed of 5% clay. Thus, a loss of adhesion of 16% is noted for a substitution of 5% whereas the substitution of cement of 10% reduces the adhesion drop to 10%. At the same time, the slip of the bar at maximum stress goes from 1.76 mm for the reference to 0.56 mm for 5% attapulgite and 1.01 mm for 10% attapulgite addition. An agreement with the work of Rashiddadash *et al.* (Reference [22]), who observed a reduction in steel-concrete bond of 18.56% for a 10% substitution of Metakaolin, was found.

The increase in slope observed for reinforced concrete containing clay is related to the cohesion between the steel and the concrete. Indeed, at the end of the first phase, the cohesion gradually breaks down with the increase of the load. The concrete located between the ribs compresses against the displacement of the reinforcement. We thus observe an increase in the mechanical interactions
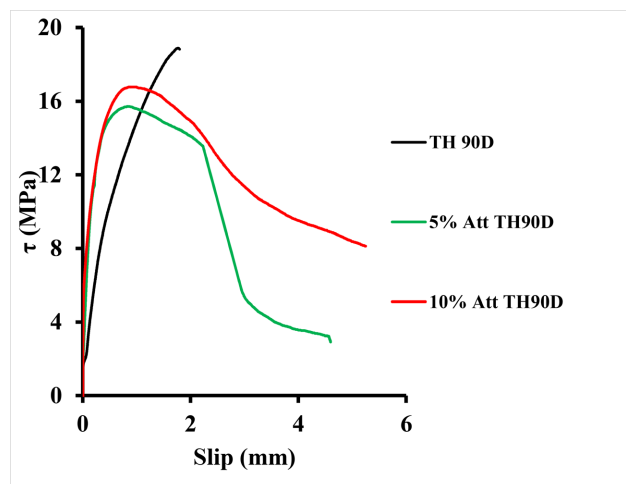

Figure 11. Effect of attapulgite on the evolution of the pull-out stress.

between the concrete and the ribs (see Reference [25]), which are more important in the absence of clay. This explains the fact that the bond stress is higher for clay-free concretes. **Figure 12** shows the evolution of the load as a function of time, associated with the acoustic activity during the loading and integrated over 3.5 second periods.

These results show that the evolution of the acoustic activity takes place in four phases during the loading, as shown in **Figure 13**.

The first phase (loads less than or equal to 25% of the maximum load) is a "silent" phase where no significant event is recorded, except for weak micro noises of crushing of the concrete under the support plate. This phase is almost non-existent
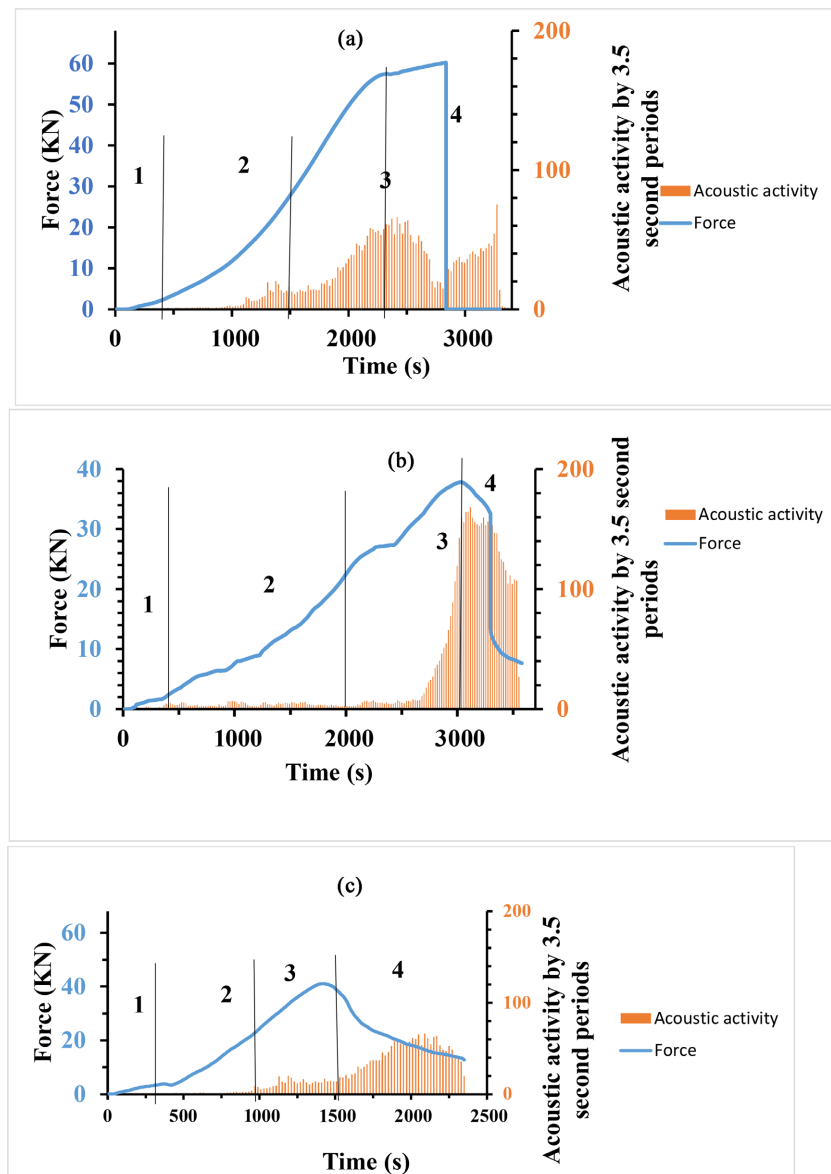
Figure 12. Evolution of the load as a function of time, associated with the acoustic activity of reinforced concrete containing or not clay and not corroded: (a) Reference; (b) 5% attapulgite and (c) 10% attapulgite.
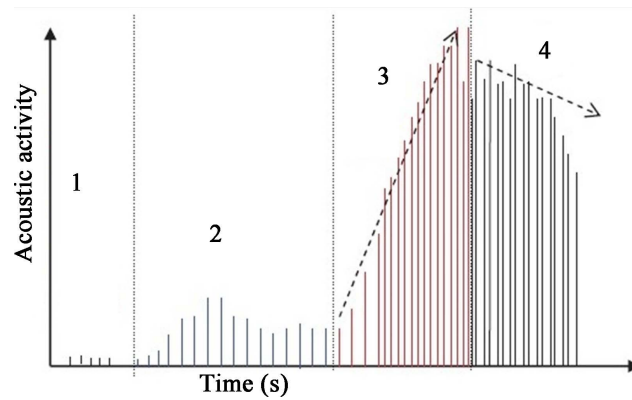
Figure 13. Evolution of acoustic events during loading (see Reference [19] [26]).

for all compositions. The second phase (between 25 and 45% of the maximum load) corresponds to the settlement and crushing of the concrete on the voids present in the specimen at the level of the upper anchorage point, generating an initiation of microcracks within the specimen. The acoustic activity in this phase is well marked for TH 90D specimens, less clear for attapulgite-based specimens and almost non-existent for attapulgite-based reinforced concrete. Indeed, this phase marks the beginning of the decohesion between the bar and the concrete. Micro-cracks are initiated and the acoustic benefits increase with this effect. This phase is associated with the first slope of the stress-slip curve (Figure 11). The evolution of the acoustic activities confirms the results of the pull-out tests showing that the presence of attapulgite increases the cohesion between the bar and the concrete. The third phase (from 45% of the maximum load to the peak of the load) corresponds to the progressive micro-cracking of the specimen and the propagation of the interface disbonding. Acoustic activity is initially low (corresponding to crack propagation), then increases rapidly until the maximum loading is reached (corresponding to interface disbonding). The acoustic activity in this phase is more pronounced in the case of concrete with 5% attapulgite. This shows that the bond between the bar and the concrete degrades more rapidly after their decohesion for the concrete with 5% clay. In the fourth phase, which starts near loading peak, the bar begins to slip, which produces numerous frictional micro-noises at the interface and crushing micro-noises of the concrete between the ribs. This phase is often short when the failure is sudden. The acoustic activity is very important and very energetic because of the micro noises due to friction.

4. Conclusions

Our study has confirmed the possibility of using attapulgite from the Thies region in Senegal as a partial substitute for cement. It was calcined at 800°C and used as a cement substitute in the preparation of concrete and reinforced concrete at contents of 0%, 5% and 10%.

The results showed that the partial substitution of calcined attapulgite for ce-

ment up to 10% does not have a significant influence on the porosity and permeability of the concrete. Compression tests indicate a low compressive strength and Young modulus of clay-based concretes in the short term. In contrast, in the long term (90 days of maturation), the compressive strength and Young modulus of the clay-based concretes increase by 6.7% and 11.0% for 5% and 10% attapulgite, respectively. This increase was confirmed by thermogravimetric analysis measurements showing a pozzolanic reactivity of attapulgite after 28 days. A loss of 16% bond is noted for a 5% substitution; while the 10% substitution caused a 10% drop in bond. The acoustic emission bond study confirmed the results of the bond tests and revealed four concrete deformation processes during loading.

However, the investigations are not exhausted and may be pursued examining percentages of substitution of attapulgite for cement higher than 10%, and other indicators of durability of steel concrete, such as electrical resistivity, shrinkage, creep and transfer properties of clay-based concrete. It would also be interesting to analyze attapulgite as a corrosion inhibitor for reinforced concrete. It is important to note that fresh concrete properties, such as setting time and measured heat of hydration of concrete, have not been considered in this document.

Acknowledgements

Conflicts of Interest

The authors declare no conflicts of interest regarding the publication of this paper.

References

[1] Plaza, P., Sáez del Bosque, I.F., Frías, M., Sánchez de Rojas, M.I. and Medina, C. (2021) Use of Recycled Coarse and Fine Aggregates in Structural Eco-Concretes. Physical and Mechanical Properties and CO_2 Emissions. *Construction and Building Materials*, **285**, Article ID: 122926.

[2] Musbau, K.D., Kolawole, J.T., Adewumi Babafemi, J. and Olalusi, O.B. (2021) Comparative Performance of Limestone Calcined Clay and Limestone Calcined Laterite Blended Cement Concrete. *Cleaner Engineering and Technology*, **4**, Article ID: 100264. https://doi.org/10.1016/j.clet.2021.100264

[3] Du, H. and Pang, S.D. (2020) High-Performance Concrete Incorporating Calcined Kaolin Clay and Limestone as Cement Substitute. *Construction and Building Materials*, **264**, Article ID: 120152. https://doi.org/10.1016/j.conbuildmat.2020.120152

[4] Liu, J., Qiu, J., Wu, P., Sun, X., Zhang, S. and Guo, Z. (2021) Calcined Oil Shale Residue as a Supplementary Cementitious Material for Ordinary Portland Cement.

Construction and Building Materials, **306**, Article ID: 124849.
https://doi.org/10.1016/j.conbuildmat.2021.124849

[5] Liu, Y., Ling, T.-C., Wang, M. and Wu, Y.-Y. (2021) Synergic Performance of Low-Kaolinite Calcined Coal Gangue Blended with Limestone in Cement Mortars. *Construction and Building Materials*, **300**, Article ID: 124012.
https://doi.org/10.1016/j.conbuildmat.2021.124012

[6] Zhuang, W., Li, S. and Yu, Q. (2022) The Effect of Supplementary Cementitious Material Systems on Dynamic Compressive Properties of Ultra-High Performance Concrete Paste. *Construction and Building Materials*, **321**, Article ID: 126361.
https://doi.org/10.1016/j.conbuildmat.2022.126361

[7] Sousa, V. and Bogas, J.A. (2021) Comparison of Energy Consumption and Carbon Emissions from Clinker and Recycled Cement Production. *Journal of Cleaner Production*, **306**, Article ID: 127277. https://doi.org/10.1016/j.jclepro.2021.127277

[8] Mascarin, L., Ez-zaki, H., Garbin, E., Bediako, M. and Valentini, L. (2022) Mitigating the Ecological Footprint of Alkali-Activated Calcined Clays by Waste Marble Addition. *Cement and Concrete Composites*, **127**, Article ID: 104382.
https://doi.org/10.1016/j.cemconcomp.2021.104382

[9] Miller, S.A., Habert, G., Myers, R.J. and Harvey, J.T. (2021) Achieving Net Zero Greenhouse Gas Emissions in the Cement Industry via Value Chain Mitigation Strategies. *One Earth*, **4**, 1398-1411. https://doi.org/10.1016/j.oneear.2021.09.011

[10] Bodian, M., Keinde, D., Touré, A.O., Gueye, P.M. and Fall, M. (2018) Valorization of Pout Attapulgite as Corrosion Inhibitor for Fe500-3 Concrete Reinforcing Iron in the Interstitial Solution of Concrete. *International Journal of Innovation and Applied Studies*, **24**, 1603-1613.

[11] Vejmelkova, E., Pavlikova, M., Keppert, M., Keršner, Z., Rovnaníková, P., Ondrácek, M. and Ellipsis, R. (2010) High Performance Concrete with Czech Metakaolin: Experimental Analysis of Strength, Toughness and Durability Characteristics. *Construction and Building Materials*, **24**, 1404-1411.
https://doi.org/10.1016/j.conbuildmat.2010.01.017

[12] Amandine, R., Annabelle, P.-M., Christophe, L. and Laurent, M. (2015) Procédé d'activation des sols argileux. HAL Id: hal-01167599.
https://hal.archives-ouvertes.fr/hal-01167599

[13] Norme Française NF EN 10080 (2005) Acier pour l'armature du béton.

[14] Norme Française NF EN 196-9, in Sogbossi, H., Verdier, J. and Multon, S. (2019) New Approach for the Measurement of Gas Permeability and Porosity Accessible to Gas in Vacuum and under Pressure. *Cement and Concrete Composites*, **103**, 59-70.
https://doi.org/10.1016/j.cemconcomp.2019.04.032

[15] Norme française NF XP P18-463 (2005) Essai de perméabilité aux gaz sur le béton durci.

[16] Klinkenberg, L.-J. (1941) The Permeability of Porous Media to Liquid and Gases, Drilling and Production Practice. American Petroleum Institute, Washington DC, 200-213.

[17] Salih, C., Manalo, A., Ferdous, W., Yu, P., Abousnina, R., Heyer, T. and Schubel, P. (2021) Effect of Bending and Compressive Modulus of Elasticity on the Behaviour of Timber-Alternative Railway Sleepers Supported by Ballast. *Case Studies in Construction Materials*, **15**, e00597. https://doi.org/10.1016/j.cscm.2021.e00597

[18] Boughezala, M.L. and Larbi, M. (2020) Comportement des colonnes en béton armé chargées axialement et soumises à des charges d'impact transversales. Diss., Univer-

sité de Batna, Batna, 2.

[19] Nguyen, N.H. (2014) Dégradation du béton armé sous actions sévères: Etude du comportement résiduel de l'adhérence à l'aide de la technique d'émission acoustique. Thèse de doctorat, INSA Rennes, Rennes.

[20] Ming, M., Zheng, S., Zhang, Y., Zheng, Y., Yang, S. and Song, M. (2021) Experimental Study on the Bond-Slip Behavior and Stress Transfer Mechanism between Shaped Steel and High-Performance Fiber-Reinforced Concrete. *Structures*, **34**, 5013-5028. https://doi.org/10.1016/j.istruc.2021.09.014

[21] Li, X., Zhang, J., Liu, B., Jiang, H. and Min, X. (2021) Bond Stress Distribution Analysis between Non-Prestressed Steel Strand and Concrete in Novel Beam-to-Column Connection. *Engineering Structures*, **242**, Article ID: 112523. https://doi.org/10.1016/j.engstruct.2021.112523

[22] Rashiddadash, P., Ramezanianpour, A.A. and Mahdikhani, M. (2014) Experimental Investigation on Flexural Toughness of Hybrid Fiber Reinforced Concrete (HFRC) Containing Metakaolin and Pumice. *Construction and Building Materials*, **51**, 313-320. https://doi.org/10.1016/j.conbuildmat.2013.10.087

[23] Benaissa, M., Bendani, K., Belas, N., Belguesmia, K. and Missoum, H. (2016) Effet de l'ajout de la bentonite sur les propriétés des mortiers et des bétons autoplaçants. *Materials and Technology*, **104**, 608. https://doi.org/10.1051/mattech/2017021

[24] Wang, Y., Shi, C., Ma, Y., Xiao, Y. and Liu, Y. (2021) Accelerators for Shotcrete—Chemical Composition and Their Effects on Hydration, Microstructure and Properties of Cement-Based Materials. *Construction and Building Materials*, **281**, Article ID: 122557.

[25] Belhimer, I. (2020) Caractérisation microstructurale, mécanique et électrochimique de l'acier rond à béton du complexe sidérurgique Algerian-Qatari Steel (AQS) d'El Milia. Thèse de doctorat. Université de Jijel, Jijel.

[26] Cao, A., Jing, G., Ding, Y.L. and Liu, S. (2019) Mining-Induced Static and Dynamic Loading Rate Effect on Rock Damage and Acoustic Emission Characteristic under Uniaxial Compression. *Safety Science*, **116**, 86-96. https://doi.org/10.1016/j.ssci.2019.03.003